Ultrafast spectroscopic investigation of a fullerene poly(3-hexylthiophene) dyad

Natalie Banerji, Jason Seifter, Mingfeng Wang, Eric Vauthey, Fred Wudl, and Alan J. Heeger

Ultrafast spectroscopic investigation of a fullerene poly(3-hexylthiophene) dyad

Natalie Banerji, Jason Seifter, Mingfeng Wang, Fred Wudl, and Alan J. Heeger*

Center for Polymers and Organic Solids, University of California, Santa Barbara, California 93106-5090, USA

Eric Vauthey

Department of Physical Chemistry, University of Geneva, 30 Quai Ernest-Ansermet, CH-1211 Geneva 4, Switzerland

Abstract

We present the femtosecond spectroscopic investigation of a covalently linked dyad, PCB-P3HT, formed by a segment of the conjugated polymer P3HT (regioregular poly(3-hexylthiophene) that is end-capped with the fullerene derivative PCB ([6,6]-phenyl-C_{61}-butyric acid ester), adapted from PCBM. The fluorescence of the P3HT segment in tetrahydrofuran (THF) solution is reduced by 64% in the dyad compared to a control compound without attached fullerene (P3HT-OH). Fluorescence up-conversion measurements reveal that the partial fluorescence quenching of PCB-P3HT in THF is multiphasic and occurs on an average time scale of 100 ps, in parallel to excited-state relaxation processes. Judging from ultrafast transient absorption experiments, the origin of the quenching is excitation energy transfer from the P3HT donor to the PCB acceptor. Due to the much higher solubility of P3HT compared to PCB in THF, the PCB-P3HT dyad molecules self-assemble into micelles. When pure C_{60} is added to the solution, it is incorporated into the fullerene-rich center of the micelles. This dramatically increases the solubility of C_{60}, but does not lead to significant additional quenching of the P3HT fluorescence by the C_{60} contained in the micelles. In PCB-P3HT thin films drop-cast from THF, the micelle structure is conserved. In contrast to solution, quantitative and ultrafast (<150 fs) charge separation occurs in the solid-state films and leads to the formation of long-lived mobile charge carriers with characteristic transient absorption signatures similar to those that have been observed in P3HT:PCBM bulk heterojunction blends. While π-stacking interactions between neighboring P3HT chains are weak in the micelles, they are strong in thin films drop-cast from *ortho*-dichlorobenzene (DCB). Here, PCB-P3HT self-assembles into a network of long fibers, clearly seen in AFM images. Ultrafast charge separation occurs also for the fibrous morphology, but the transient absorption experiments show fast loss of part of the charge carriers due to intensity-induced

recombination/annihilation processes and monomolecular interfacial trap-mediated or geminate recombination. The yield of the long-lived charge carriers in the highly organized fibers is however comparable to that obtained with annealed P3HT:PCBM blends. PCB-P3HT can therefore be considered as an active material in organic photovoltaic devices.

I. INTRODUCTION

In organic solar cells, charge carriers are generated by photoinduced charge separation (CS) at the heterojunction between an electron donor (D) and an electron acceptor (A).[1] Conjugated polymers are typical electron donors that are blended with an electron-accepting fullerene derivative, such as PCBM ([6,6]-phenyl-C_{61}-butyric acid methyl ester), to yield a bulk heterojunction (BHJ) material.[2-5] The nanoscale morphology in the BHJ ensures a high D-A interface for efficient CS and phase-separated fullerene and polymer networks for charge transport to the electrodes. Another approach to obtain long-lived CS, often used with small or oligomeric molecules, is to covalently link the donor and acceptor, either directly, via a bridge or in a highly sophisticated architecture of several D and A units.[6-13] For photovoltaics, appropriate molecular design is frequently assisted by supramolecular assembly into the desired active layer structure. Control over functionality and morphology can thus be achieved, for example by introducing a redox gradient for optimal light and charge funnelling,[14-21] or by devising an organized BHJ.[22-24]

Dyads or triads consisting of a conjugated oligomer with 2-5 repeat units, such as oligothiophene or oligo(p-phenylene vinylene), attached to a fullerene derivative have been reported.[25-31] They are typically used as model compounds in photophysical studies. Singlet excitation energy transfer (EET) often competes with CS, especially in non-polar solution and for short oligomers. Charge carriers can nevertheless be formed upon photoexcitation for longer oligomer chains in polar solvents and in thin films,[27, 29-31] although it has been suggested in some cases that EET from the oligomer to the fullerene precedes the CS step. [29, 30] In thin films, the carrier lifetime can extend to the millisecond regime,[29, 30] and supramolecular organization is possible, for example to form a fibrous nanostructure.[26]

Nevertheless, the efficiency of photovoltaic devices made with oligomer-fullerene compounds remains low.[26, 27, 29, 30]

Some attempts have also been made to covalently link conjugated polymers to fullerene derivatives, but so far the single component systems have had less success in photovoltaic devices than BHJ blends of the separate D and A. One approach consists in grafting several pendant fullerenes onto the polymer backbone in so-called "double cable" polymers.[28, 32, 33] The occurrence of photoinduced CS and formation of long-lived mobile charge carriers was for example demonstrated by Cravino et al. using photoinduced absorption and light-induced electron spin resonance measurements for a double cable polymer having a bithiophene repeat unit with an attached fulleropyrrolidine group.[34, 35] A solar cell made using a double cable compound with a hybrid poly(p-phenylene vinylene)/poly(p-phenylene ethynylene) backbone and attached methanofullerenes was first reported by Janssen and co-workers.[36] Singlet EET to the fullerene was found to occur in non-polar solution, while the polymer fluorescence was quenched by photoinduced CS in thin films, yielding charge carriers with a millisecond lifetime. Instead of having a fullerene moiety attached on every repeat unit, a random copolymerization of monomers containing attached fullerenes and monomers with for example solubilizing side chains has been attempted.[37]

Better control of the nano-phase separation in films, though with less efficient CS, was observed in a polythiophene-based diblock copolymer where one block comprises the fullerenes, compared to the corresponding polymer with a random sequence of the electron donor and acceptor.[38] There are several other examples of supramolecular assembly in block copolymers. A poly(p-phenylene vinylene)/C_{60}-polystyrene system yields a honeycomb pattern morphology if cast from carbon disulfide and micro-phase separation if cast from chloroform (efficient fluorescence quenching and better photovoltaic response than in a blend of the constituent polymers was observed).[39, 40] Compounds based on P3HT (regioregular poly(3-hexylthiophene) are capable of forming nanofibrils.[41, 42] Also, a multiblock copolymer with C_{60} groups directly incorporated into the backbone was reported, where morphologies ranging from micelles to wires were obtained depending on the processing conditions.[43] While the efficiency of photovoltaic devices containing solely a block copolymer in the active layer remains low,

such compounds have been successfully added as "surfactants" to BHJ blends. Thus, the morphology of P3HT:PCBM active layers could be stabilized against large scale phase separation due to thermal treatment by addition of a diblock copolymer containing a fullerene part and a P3HT part.[44] Also, a P3HT/C_{60} rod-coil diblock copolymer reported by Wudl and co-workers increased P3HT:PCBM solar cell efficiency by up to 35% if added in small amounts.[41]

Conjugated polymers that are end-capped by a fullerene derivative are much less common. Guldi and co-workers reported compounds in which a C_{60}-acceptor is covalently linked to a tetrathiafulvalene-donor via a short poly(p-phenylenevinylene) wire, which does not, however, actively participate in the CS process.[45, 46] Boudouris et al. synthesized a C_{60}-P3HT-C_{60} polymer and observed micro-phase separation in thin films into semicristalline P3HT and fullerene domains.[47] However, no further photovoltaic study or detailed photophysical characterization was undertaken. It is particularly interesting to work with P3HT, as power conversion efficiencies around 5% can be obtained with thermally annealed P3HT:PCBM blends.[3, 48-50] Furthermore, the strong interchain interactions of P3HT allow a microcrystalline film morphology where the polymer chains π-stack into two-dimensional lamellar sheets.[51] It can therefore be expected that covalently linked dyads of P3HT and PCBM have photovoltaic potential with control over the CS and charge recombination (CR) processes, while the C_{60} end-capping is less likely to disrupt this supramolecular assembly of P3HT compared to polymers with fullerenes attached along the chain.

The synthesis of the PCB-P3HT dyad shown in Fig. 1(a) has recently been reported independently by Wang et al.[52] and Lee et al.[53] Here, a polymer chain of about 30 repeat units is covalently attached to a fullerene derivative (PCB) adapted from PCBM. Significant self-organization, strongly dependent on processing conditions, was observed in both solution and thin films.[52] In particular, PCB-P3HT forms micelles in tetrahydrofuran (THF), a solvent with selective solubility for P3HT. Additional C_{60} can be incorporated into the fullerene-rich center of the micelles, which dramatically increases the solubility of C_{60} in THF. A micellar morphology is also obtained in thin films cast from THF. On the other hand, a nano-scale fibrous morphology is obtained in films cast from *ortho*-dichlorobenzene (DCB), with promise for formation of a controlled BHJ for applications in photovoltaic devices. PCB-

4

P3HT has also been used as a surfactant added in small amounts to P3HT:PCBM blends.[53] The domain size of the P3HT and PCBM regions in the film could thus be reduced and large-scale phase-separation could be prevented, even after prolonged thermal annealing.

We report here on the photophysical characterization of PCB-P3HT. The dyad was investigated in THF solution, with and without additional C_{60}, using steady-state spectroscopy as well as femtosecond-resolved fluorescence up-conversion and transient absorption (TA) spectroscopy. The CS and CR processes were then compared for thin films drop-cast from either THF or DCB using ultrafast TA spectroscopy, in order to understand the effects of the morphology (micelles versus fibrous network). We expected that improved transport in the fibrous morphology would increase the yield and lifetime of the charge carriers. To be certain of the morphology of the thin-film samples used, tapping mode atomic force microscopy (TMAFM) was carried out. In parallel to all experiments, measurements were performed with the control system P3HT-OH shown in Fig. 1(b), which is the synthetic precursor of PCB-P3HT without the attached PCB.

II. EXPERIMENTAL METHODS

A. Samples

P3HT-OH and PCB-P3HT were synthesized according to the method previously described,[52] PCBM was prepared by the usual procedure and C_{60} was obtained from SES Inc. For the solution characterizations, the molecules were dissolved in anhydrous THF, CS_2 or a mixture of the two, as specified throughout the text. Steady-state spectroscopy was typically carried out in a 1 cm quartz cell with a concentration of P3HT-OH or PCB-P3HT of ≤ 0.05 mg/mL (~ 0.01 mg/mL for fluorescence experiments to avoid re-absorption with an optical density in the visible of < 0.2). Unless specified otherwise, the P3HT-OH and PCB-P3HT concentrations for the fluorescence up-conversion measurements were 1 mg/mL and 2 mg/mL, respectively. The solutions were placed in a 0.25 mm cell which consisted of two Spectrosil® quartz disks separated by a Teflon spacer. The optical density at the excitation wavelength (500 nm) was 0.5-0.6. A 1 mm cell was used for more dilute solutions. For TA experiments in THF solution, a concentration of P3HT-OH and PCB-P3HT of the order of 0.5

mg/mL was used, giving an optical density at the excitation wavelength (400 nm) in a 1 mm quartz cell of 1.5 and 1.3, respectively. For thin film TA measurements, P3HT-OH was drop-cast in a nitrogen glovebox from THF (2 mg/mL) on a sapphire substrate. The visible absorption maximum of the P3HT band (475 nm) had an optical density of 0.53. PCB-P3HT was drop-cast either from THF (2 mg/mL) or from DCB (12 mg/mL). In the latter case, slow drying at room temperature ensured formation of the wanted fibrous morphology. Thinner films than with P3HT-OH were obtained for PCB-P3HT, with a maximum absorbance due to the P3HT segment around 0.15 for both samples.

B. Steady-state spectroscopy

Steady-state absorption spectra were measured with a Cary 50 (Varian) spectrophotometer, while fluorescence emission and excitation spectra were recorded with a Cary Eclipse (Varian) fluorimeter. All fluorescence spectra were corrected for the wavelength-dependent sensitivity of the detection. To compare the fluorescence quantum yield of P3HT-OH and PCB-P3HT, solutions in THF were prepared that had almost the same absorbance at the excitation wavelength of 500 nm and their emission spectra were recorded in similar conditions. As a relative measure of the fluorescence quantum yield, the area of the spectra was obtained by integration and corrected for small variations in absorbance at the excitation wavelength.

C. Fluorescence up-conversion spectroscopy

Emission dynamics on the femtosecond time scale were obtained in solution using the fluorescence up-conversion setup previously described.[54, 55] In brief, the 1000 nm output of a tunable Mai Tai HP (Spectra-Physics) mode-locked Ti:sapphire laser system (100 fs pulse duration, 80 MHz repetition rate) was frequency doubled for sample excitation at 500 nm. The pump power was 3 mW with a spot diameter of about 20 μm on the sample. The measured sample fluorescence was detected by sum-frequency generation with a delayed gate pulse, then the up-converted signal was dispersed in a monochromator and its intensity measured with a photomultiplier tube. The polarization of the pump beam was at magic angle (54.7°) relative to that of the gate pulses, except for polarization-sensitive measurements where it was set to 0° (parallel) and 90° (perpendicular). Measurements were done at room temperature in ambient conditions. To minimize degradation, the sample cell was constantly

rotated during the measurement. Three scans of the dynamics in the -5 ps to 1500 ps range were averaged at each emission wavelength.

The time-resolved emission data were analyzed using the sum of exponential functions convoluted with a Gaussian-shaped instrument response function (IRF). In order to reconstruct time-resolved emission spectra, a global analysis was undertaken, as described in detail elsewhere.[54, 56] In brief, for each sample the normalized fluorescence time profiles at various emission wavelengths were analyzed globally using the convolution of a Gaussian-shaped IRF with the sum of exponential terms. The width of the IRF was typically around 140 fs for solution measurements with the 0.25 mm cell. The wavelength-dependent amplitudes (or pre-exponential factors) were scaled to the steady-state emission spectrum, assuming that the steady-state emission intensity at a given wavelength is the time integral of the corresponding emission time profile. The time-resolved emission spectra were then reconstructed using the analytical expression for the time profiles at different wavelengths with the parameters (time constants and scaled amplitudes) from the fitting procedure. For femtosecond-resolved fluorescence anisotropy measurements, the anisotropy decay, r(t), was calculated from the FU time profiles with the polarization of the pump beam parallel and perpendicular with respect to the gate beam, using the standard equation. This r(t) was analyzed using the sum of exponential terms.

D. Transient absorption spectroscopy

TA spectra were recorded for dissolved samples and drop-cast solid samples using femtosecond pulsed laser pump-probe spectroscopy. The 400 nm pump beam was generated by frequency doubling the 800 nm output of a Ti:sapphire laser system with a regenerative amplifier providing 100 fs pulses at a repetition rate of 1 kHz. The pump intensity per pulse was around 45 $\mu J/cm^2$ for the solution measurements and 190 $\mu J/cm^2$ for the film measurements. The probe beam in the visible and near-infrared range (400-1100 nm) consisted of a white light continuum, generated by passing a portion of the 800 nm amplified Ti:sapphire output through a 1 mm thick sapphire plate. The probe intensity was always less than the pump intensity and the spot size was much smaller. The probe pulses were time delayed with respect to the pump pulses using a computerized translation stage. The probe beam was split before the sample into a signal beam (transmitted through the sample and crossed with the pump

beam) and a reference beam. The signal and reference were detected with a pair of 163 mm spectrographs (Andor Technology, SR163) equipped with a 512×58 pixels back-thinned CCD (Hamamatsu S07030-0906) and assembled by Entwicklungsbüro Stresing, Berlin. To improve sensitivity, the pump light was chopped at half the amplifier frequency, and the transmitted signal intensity was recorded shot by shot. It was corrected for intensity fluctuations using the reference beam. The transient spectra were averaged until the desired signal-to-noise ratio was achieved. The polarization of the probe pulses was at magic angle relative to that of the pump pulses. All spectra were corrected for the chirp of the white-light probe pulses. The FWHM of the response function was about 150 fs. The solution samples were constantly bubbled with inert gas during the TA measurements to provide stirring and to remove oxygen, while the solid samples were kept under dynamic vacuum (<10^{-4} mbar). All TA dynamics were analyzed using the sum of exponential terms.

E. AFM microscopy

To characterize the thin film morphology of the solid samples used in transient absorption spectroscopy, tapping mode atomic force microscopy (TMAFM) was carried out at room temperature in air with an MFP-3D-SA Atomic Force Microscope made by Asylum Research. The probes were FORTA probes from Applied Nanostructures, which have a silicon cantilever of nominal spring constant 3.0 N/m, a nominal resonance frequency of ~60 kHz, and which were tuned to an RMS cantilever oscillation amplitude of ~1000 mV. Acquired images were 1 × 1 μm, taken with a scan frequency of 1 Hz.

III. RESULTS AND DISCUSSION

A. PCB-P3HT in solution (steady-state spectra and time-resolved emission)

The steady-state absorption spectra of PCB-P3HT, P3HT-OH and PCBM in THF solution are shown in Fig. 2(a). The spectrum of the dyad is clearly the superposition of its constituents, indicating the absence of any electronic interaction or charge transfer between the donor and acceptor in the ground state. The weak electronic coupling between the PCB and P3HT moieties can be explained by the rather long and non-conjugated linker. Through-space interactions due to folding of the molecule

and aggregation of the two parts can also be excluded. The absorption spectrum of P3HT-OH in THF solution is broad and structureless, typical for non-aggregated P3HT chains.[57, 58] For PCB-P3HT, the small shoulders at 410 nm and 430 nm are due to PCB and are not due to any structure in the P3HT absorption, so that it can be concluded that π-stacking of the polymer chains is not significant for the dyad in THF. The results are in agreement with the previously proposed self-assembly of PCB-P3HT in THF into micelles.[52] As P3HT is much more soluble in THF than PCB, the fullerenes are found on the inside of the micelles while the non-aggregated P3HT chains are in contact with the solvent.

The fluorescence spectra of P3HT-OH and PCB-P3HT in THF are also shown in Fig. 2(a). They were recorded upon 500 nm excitation (mainly of the P3HT moiety in the dyad) with solutions that had a similar absorbance at this wavelength. The shape of the spectra is the same for the two compounds, indicating that the fluorescence in the dyad stems essentially from the P3HT moiety. As is typical for this polymer, the structured P3HT emission spectrum is not the mirror image of the absorption. The absorption of P3HT is a π-π^* interband transition, while emission occurs from a relaxed singlet exciton state.[58] The fluorescence excitation spectrum of PCB-P3HT in THF recorded at the emission maximum differs from the corresponding absorption spectrum (Fig. 2(a)), mainly because there is no contribution from the PCB moiety. This shows that the observed emission results exclusively from P3HT and not PCB excitation. The excitation spectrum is nevertheless close but not precisely equal in shape to the P3HT absorption spectrum, as shown by comparison to the P3HT-OH control compound (Fig. 2(a)). We recently ascribed a similar difference between the absorption and excitation spectrum of P3HT polymer in solution to torsional disorder of the polymer, with some conformations having a higher fluorescence quantum yield than others.[58]

Even if the shape of the emission spectra of P3HT-OH and PCB-P3HT is the same, the fluorescence intensity of the dyad is reduced by 64% (Fig. 2(a)). This indicates that the emission of the P3HT segment is quenched by the presence of PCB. In order to find the rate associated with the quenching process, time-resolved emission measurements with a femtosecond resolution were carried out following 500 nm excitation. The fluorescence time profiles of P3HT-OH and PCB-P3HT recorded in THF solution at the emission maximum (575 nm) are compared in Fig. 3(a). At this wavelength,

effects of spectral relaxation (discussed below) are small, so that the dynamics represent mainly the decay of the singlet exciton. For P3HT-OH, the time profile at 575 nm is dominated by a 550 ps time constant, in excellent agreement with the value previously reported for exciton decay of P3HT polymer in solution.[58] Due to quenching with PCB, the decay of the 575 nm emission in PCB-P3HT is faster and multiphasic with time constants of 5.1 ps (18%), 65.5 ps (27%) and 447 ps (55%). As shown in Fig. 3(a), this emission dynamics in the dyad does not change if a much more dilute solution is used (0.05 mg/mL versus 2 mg/mL) or if it is dissolved in a solvent mixture containing THF and less polar carbon disulfide (CS_2) in a 3:1 ratio. The presence of the ~500 ps time constant in both P3HT-OH and PCB-P3HT suggests that the fluorescence of the P3HT moiety in the dyad is only partially quenched by the attached PCB. Indeed, the 575 nm emission time profiles of P3HT and PCB-P3HT converge after 550 ps if the are scaled at long timedelay (Fig. 2(b)). In order to extract the dynamics related only to the quenching process in PCB-P3HT (without the non-quenched contribution to the emission), we subtracted the scaled time profile of P3HT-OH from that of the dyad. As shown in Fig. 2(b), the 'difference' time profile can be reproduced with time constants of 2.1 ps (20%), 23.6 ps (30%) and 187 ps (50%). It can therefore be concluded that quenching in the PCB-P3HT dyad occurs with a distribution of time constants on an average time scale of 100 ps.

There is a strong dependence of the early fluorescence time profiles of P3HT-OH and PCB-P3HT in THF on the emission wavelength, as shown for the dyad in Fig. 3(c). The observed fast decay at short wavelengths and rise at long wavelengths is typical for spectral changes, such as a red shift, that are brought about by excited-state relaxation and which contribute to the fluorescence dynamics in addition to exciton decay. In order to characterize the spectral changes, the time profiles recorded throughout the emission spectrum were analyzed globally using the sum of exponential terms convoluted with the instrument response. For P3HT-OH dissolved in THF, time constants of $\tau_1 = 0.6$ ps, $\tau_2 = 8.6$ ps, $\tau_3 = 41$ ps and $\tau_4 = 553$ ps were found. This is in excellent agreement with the outcome of a similar analysis of the emission time profiles of P3HT polymer in chlorobenzene solution.[58] The first three time constants are ascribed to spectral relaxation, while the long one represents the decay of the relaxed singlet exciton. We interpret the rather complex excited-state relaxation processes in P3HT

and P3HT-OH within the following model:[54, 58] Following interband absorption in the conjugated polymer, the primary photoexcitation self-localizes within ~100 fs and a bound exciton is formed on the 1 ps time scale. Consecutive exciton hopping steps as well as planarization of the polymer backbone by torsional relaxation then continue for several tens of picoseconds, leading to the observed spectral relaxation.

The global time constants found for PCB-P3HT in THF solution are $\tau_1 = 0.7$ ps, $\tau_2 = 7.8$ ps, $\tau_3 = 95$ ps and $\tau_4 = 496$ ps. As discussed earlier, quenching of the P3HT emission by the attached fullerene occurs over several time scales ranging from ~2 ps to ~200 ps. This implies that the quenching takes place in parallel to the excited-state relaxation, so that both multiphasic phenomena contribute to the global time constants. The amplitude spectra associated with the time constants are shown in the inset of Fig. 2(b). The first two amplitude spectra suggest a decay at short wavelengths (positive amplitude) and a rise at long wavelengths (negative amplitude), typical for spectral dynamics. The spectra associated with τ_3 and τ_4 are all-positive and close to the steady-state emission spectrum, suggesting a strong contribution from exciton decay. It is however impossible to completely disentangle the quenching dynamics from the relaxation dynamics using the global analysis or any other reasonable model. The outcome of the global analysis is nevertheless useful to reconstruct the time-resolved emission spectra. The spectral changes due to relaxation processes can then be clearly observed in the normalized spectra, shown for PCB-P3HT in Fig. 2(b). There is a narrowing on the blue side of the spectrum mainly due to exciton hopping to lower energy between segments in the P3HT chain that are formed by breaks in the conjugation (disorder). The important growth of the 0-1 vibronic shoulder at 620 nm, which is absent at the earliest time delays, is ascribed to changes in the selection rules for this transition brought about by the planarization of the P3HT chain in the excited state. It should be noted that spectral relaxation in the dyad takes longer than in P3HT-OH, probably because the bulky fullerene group slows down torsional relaxation. The fully relaxed (steady-state) fluorescence spectrum is reached after 50 ps in the control compound, but only after 300 ps in PCB-P3HT.

Finally, the time-resolved polarization anisotropy of the 575 nm fluorescence is compared for P3HT-OH and PCB-P3HT in THF in Fig. 3(d) and it can be seen that the anisotropy decays are very

similar. The initial anisotropy that can be measured with ~100 fs time resolution is 0.37 for both materials, close to the theoretical maximum of 0.4 for perfectly parallel absorbing and emitting transition dipole moments. For the relatively short P3HT chains (30 repeat units), this implies little depolarization during the self-localization processes that typically occur for conjugated polymers during the 100 fs following photoexcitation. The measured initial anisotropy is much lower if the delocalization of the excitation directly after the light absorption is higher, i.e. for longer polymer chains or with excitation higher into the energy bands.[58] Some fast anisotropy decay occurs during the first 100-200 ps for P3HT-OH and PCB-P3HT in solution (Fig. 3(d)), caused by the same relaxation mechanisms (exciton hopping, torsional rearrangements) that bring about the temporal evolution of the emission spectrum. The similarity of this anisotropy decay suggests a similar P3HT chain conformation (extension, coiling, folding) in the dyad micelles compared to the free P3HT-OH chains. A large geometrical difference would affect the depolarization during exciton hopping. At last, an important fraction of the anisotropy is very long-lived for both compounds (nanosecond time scale), as it decays only due to slow diffusional rotation of the entire molecules in solution.

B. PCB-P3HT in solution (femtosecond transient absorption spectroscopy)

The origin of the fluorescence quenching in the PCB-P3HT dyad could be charge separation or excitation energy transfer from the P3HT segment to the attached PCB. In order to distinguish between the two processes, transient absorption spectroscopy was carried out for P3HT-OH and PCB-P3HT in THF solution. The TA spectra at different timedelays are shown for P3HT-OH in Fig. 4(a). By comparison with the steady-state absorption spectrum, the ground state bleach (GSB) should appear as a negative signal below 500 nm. Only part of the bleach signal is nevertheless seen at 480 nm, the rest is masked by an overlapping positive band (photoinduced absorption, PIA) below 460 nm. The negative stimulated emission (SE) band can be seen as a broad and structured signature in the 590 nm region after 10 ps, in agreement with the SE spectrum calculated by multiplying the steady-state emission spectrum by λ^4 (shown as a dotted curve). At short timedelays, the SE is strongly blue-shifted (overlapping with the ground state bleach) and has a weaker relative intensity. The early spectral changes observed in the SE band are comparable to the ones described earlier in the spontaneous

emission and measured by fluorescence up-conversion. They can be ascribed to the same relaxation mechanisms in the excited state: Exciton formation, exciton hopping and polymer backbone planarization. The red-shift of the SE appears even more pronounced, probably because more excess energy is brought to the system with the 400 nm excitation used in the TA experiments than with the 500 nm excitation of the time-resolved emission measurements.

The TA spectra of P3HT-OH at high wavelengths (>700 nm) show a positive photoinduced absorption signal, with a predominant band in the 900-1000 nm region during the first hundred picoseconds. This band can be ascribed to the singlet photoexcitation, in good agreement with what has been reported in literature for P3HT in chlorobenzene.[59] Some spectral dynamics, such a shift from ~930 nm to ~970 nm and an increase in intensity, appear at early timedelays due to the excited-state relaxation. Note that the region around 800 nm is experimentally not accessible. The PIA around 970 nm and the SE disappear at long timedelays (>1 ns), while most of the GSB persists. There is a concomitant rise of a new band in the 700-900 nm region, which we assign to the triplet exciton of P3HT-OH, again in accordance with previous reports for P3HT.[59] It can be concluded that the singlet exciton in dissolved P3HT-OH, after it has formed and relaxed, undergoes mainly intersystem crossing to the long-lived triplet state.

The TA spectra for PCB-P3HT dissolved in THF, shown in Fig. 4(b), are surprisingly similar to the ones of P3HT-OH at all timedelays, except for some changes in the relative intensity of the bands. Indeed, the comparison of the normalized spectra of the two compounds at a short (0.25 ps) and at a long (~1.5 ns) timedelay in Fig. 4(c) reveals only very minor differences, especially in the region below 500 nm. In the dyad, not only the P3HT moiety, but also some of the PCB is excited at 400 nm, so that the enhanced negative signal in the 460 nm region at 0.25 ps can be assigned to the ground state bleach of the fullerene (by comparison with the steady-state spectra in Fig. 2). Nevertheless, there are no apparent spectral signatures of excited-state PCB absorption (the singlet excited state of C_{60} in toluene absorbs at 513, 759 and mostly 885 nm[60]). The bands are most probably masked by the transitions of the conjugated P3HT segment, which have much higher oscillator strength.

In order to gain more insight to the difference in photophysics between P3HT-OH and PCB-P3HT, the normalized dynamics are compared for the two compounds at different wavelengths in Fig. 5. At 1000 nm (panel (e)), the pure dynamics of the singlet PIA of the P3HT segment can be followed, since there is no triplet contribution at this wavelength. For P3HT-OH, there is a fast biphasic rise due to early relaxation processes, then the intensity decays with a ~500 ps time constant (see inset table), in good agreement with the singlet exciton decay rate obtained from the fluorescence up-conversion measurements. On the other hand, a faster decay with time constants ranging from a few picoseconds to hundreds of picoseconds is observed for the PCB-P3HT dyad, due to the partial and multiphasic quenching of the polymer segment by the fullerene. Similarly, the stimulated P3HT emission at 575 nm (panel (b)) decays faster in the presence of the attached PCB moiety, although the quenching dynamics is strongly entangled with the spectral relaxation. Note that the dynamics for both compounds and at all wavelengths scaled linearly with the pump intensity when it was varied in the 20-90 $\mu J/cm^2$ range and that the time constants remained the same, so that any intensity-dependent effects on the dynamics in Fig. 5 (measured at 45 $\mu J/cm^2$) can be excluded.

It is clear from the spectra in Fig. 4 that the triplet state is populated at long timedelays (> 1 ns) in both P3HT-OH and PCB-P3HT. This indicates that the non-quenched fraction of the dyad singlet excitons also undergoes intersystem crossing. It is difficult to extract the pure triplet state dynamics due to overlap with other spectral signatures. At 730 nm (Fig. 4 and Fig. 5(c)), the initial positive TA intensity stems from singlet PIA for both compounds. There is a fast decay within tens of picoseconds, partly due to the red shift of the negative SE signature into this spectral region, partly due to dynamics of the singlet exciton absorption itself (relaxation, quenching in the dyad). The intensity at 730 nm then increases again with a time constant of several hundred picoseconds until it reaches a plateau, which we ascribe to intersystem crossing to the triplet state. The triplet exciton plateau is much more pronounced for P3HT-OH than PCB-P3HT. At 865 nm (Fig. 4 and Fig. 5(d)), both the singlet and triplet state absorb. The fast multiexponential decay observed at this wavelength is caused by relaxation, quenching (in PCB-P3HT), and intersystem crossing of the singlet excitation. The plateau at 865 nm is due to the triplet exciton absorption and it is again more pronounced for P3HT-OH than for

the dyad. It can be concluded that the triplet state is populated in P3HT-OH and PCB-P3HT with a time constant of ~500 ps, but the triplet yield is lower in the dyad because part of the singlet excitons undergo an alternative quenching mechanism other than intersystem crossing.

It is not straightforward to assign the quenching mechanism in PCB-P3HT from the TA spectra shown in Fig. 4, since only the spectral signatures of the triplet state are seen at long timedelays and there is no sign of any additional quenching products. The observed multiphasic quenching of the P3HT singlet state in the dyad could be due to energy or electron transfer to the attached fullerene. Both processes increase the ground state bleach of the PCB moiety, which can be seen as a progressive broadening on the blue side of the negative bleach signal (~450 nm) only for PCB-P3HT (Fig. 4(b) and (c)). EET from the P3HT to the PCB moiety should also lead to an increase of the singlet excited-state absorption of the fullerene. As mentioned before, this is probably hidden by the much more intense singlet and triplet bands of the polymer segment. On the other hand, CS should lead to the appearance of the absorption bands of the positively charged P3HT polaron (intrachain polarons in P3HT polymer have a broad absorption around 950 nm[61-63]) and of the negatively charged fullerene (around 1000 nm[64]). The absence of those bands for PCB-P3HT, which have relatively high oscillator strength and do not overlap strongly with the triplet absorption, speaks against the occurrence of CS.

Furthermore, electron transfer would not cause any ground state recovery of the P3HT moiety, while the P3HT segment returns to the ground state in the case of EET to the fullerene. Indeed, the dynamics recorded in the bleach signal at 480 nm show faster ground state recovery for PCB-P3HT compared to P3HT-OH (Fig. 5(a)), pointing to energy transfer as the quenching mechanism. The effect is not as pronounced as might be expected, because of the overlapping increase of the fullerene bleach at this wavelength during the energy transfer. Note that the 480 nm signal in both compounds also has a contribution of SE at the earliest timedelays and possibly of the PIA band visible around 430 nm, which explains the rather complex dynamics at this wavelength, for example the fast initial decay during spectral relaxation. It could be argued that CS followed by ultrafast charge recombination leads to the faster ground state recovery in PCB-P3HT and to the absence of spectral signatures due to charged species (which do not have time to build up). In this case, the bleach of the PCB moiety should

however also disappear at long timedelays, contrary to the observed growth and persistence of the fullerene bleach signal around 450 nm (Fig. 4(b) and (c)). This mechanism can therefore be excluded.

We conclude that the quenching that occurs for the dyad in THF solution is caused by energy transfer from the excited P3HT moiety to the PCB moiety, rather than by charge separation. This agrees with the independence of the quenching dynamics measured by fluorescence up-conversion on the solvent polarity (no difference was observed when CS_2 was added to the solution). The multiphasic nature of the EET can be ascribed to singlet excitons that localize more or less far from the PCB on the polymer chain following the initial excitation, so that they need to migrate different distances. For the excitons that are formed furthest from the attached fullerene, no quenching occurs, instead they undergo intersystem crossing.

C. PCB-P3HT with C_{60} in solution

PCB-P3HT can act as a surfactant in solution and increase the solubility of free C_{60} molecules in solvents such as THF, by incorporating the C_{60} into the fullerene-rich center of self-assembled micelles.[52]s Figure 6(a) shows the absorption spectrum of a saturated solution of C_{60} in a THF:CS_2 solvent mixture (19:1 ratio). The fullerene concentration is of the order of 0.025 mg/mL and addition of any more C_{60} resulted in precipitation. In the same solvent mixture, 0.2 mg/mL of C_{60} (almost 10 times more) can easily be dissolved in the presence of PCB-P3HT (0.05 mg/mL). Note that CS_2 (a good solvent for fullerenes) is added to allow initial dissolution and micelle formation. The absorption spectra of this C_{60}/PCB-P3HT solution and of PCB-P3HT alone at the same concentration are illustrated in Fig. 6(a). For comparison, the slightly shifted absorption spectrum of 0.2 mg/mL C_{60} in pure CS_2 is also shown; it confirms the high concentration of dissolved C_{60} in the C_{60}/PCB-P3HT mixture. The spectrum of the latter is essentially a superposition of the spectra of C_{60} and PCB-P3HT at the same concentrations, indicating no significant aggregation effects.

Fluorescence up-conversion with 500 nm excitation was undertaken for the C_{60}/PCB-P3HT and PCB-P3HT solutions mentioned in the previous paragraph. The time profiles at the emission maximum are shown in the inset of Fig. 6(a) and are identical with and without the C_{60}. Thus, the addition of more C_{60} to PCB-P3HT in THF-rich solution does not lead to any further quenching of the P3HT

16

fluorescence. This is in excellent agreement with the proposed picture of micelle formation. As the fullerenes are found inside the micelles, they are not in direct contact with the P3HT chains and are therefore not involved in the quenching process. Finally, a solution with a very high C_{60} concentration of 2 mg/mL was prepared. An equal concentration of PCB-P3HT (2 mg/mL) and a high CS_2 proportion (THF:CS_2 3:1) had to be used to ensure solubility. The fluorescence time profile of this mixture at 575 nm is compared to the one of pure PCB-P3HT in similar conditions in Fig. 6(b). There is now a very slight additional quenching in the presence of the extra C_{60}. This is ascribed to diffusion-controlled EET of some free C_{60} molecules (not incorporated in the micelles) with the P3HT chains.

D. PCB-P3HT thin films

Thin films of PCB-P3HT were drop-cast from THF or DCB on sapphire substrates for transient absorption measurements. Again, a film of P3HT-OH, drop-cast from THF, was used as a control. AFM phase pictures of the dyad samples obtained from the two solvents are compared in Fig. 7. A globular morphology is discerned for the THF-cast film, in agreement with the micelle formation in this solvent that was discussed before. The inset of Fig. 7(a) is a schematic representation of the proposed self-assembly of PCB-P3HT into micelles. On the other hand, a fibrous network is seen in the AFM picture of the dyad cast from DCB (Fig. 7(b)). In this solvent, both P3HT and PCBM are soluble, which explains the absence of micelle formation. The proposed self-assembly into the fibers is represented in the inset of Fig. 7(b). It is driven by π-stacking of the P3HT chains, while the PCB moieties form a layer around the P3HT fibers.[52] Note that fibers due to P3HT crystallization were also seen for the P3HT-OH control sample cast from THF (data not shown). The fact that the fibrous morphology can be maintained in the dyad evidences that C_{60} end-capping does not disrupt the self-assembly of the P3HT chains.

TA spectra of the P3HT-OH film at various timedelays after 400 nm excitation are shown in Fig. 8(a). The spectra are very similar to the ones that have been reported by our group for pure P3HT film,[65] and that were interpreted according to the analysis of Vardeny and co-workers.[61, 63] The broad negative band that extends below 660 nm is due to the GSB, as it coincides spectrally with the steady-state absorption spectrum (shown as a dotted black line). There is considerable structure in the ground

state absorption of the film and it is red-shifted compared to the one obtained for P3HT-OH in solution (Fig. 2(a)). This is typical for ordering of P3HT chains into π-stacked lamellar sheets in the solid state.[58] The PIA of the P3HT-OH singlet excited state is seen as a positive signal in the 850 nm to 1050 nm region. Photoexcitation of regioregular P3HT in the solid state also leads to the direct generation of some charged polarons.[66] Delocalized polarons (in highly ordered regions) absorb around 730 nm, while localized polarons (in more amorphous regions) absorb around 950 nm.[65] For the data shown in Fig. 8(a), the positive delocalized polaron absorption thus overlaps with the negative SE band that is expected in the same spectral region, so that the bands of opposite sign cancel each other to almost no intensity around 700 nm. The localized polarons on the other hand overlap with the singlet exciton absorption at 950 nm, where a small contribution of the P3HT-OH triplet state is also expected. In general, the triplet yield for ordered regioregular P3HT films is very low compared to the isolated chains in solution.[59, 63]

Figure 9(a) shows the transient time profiles of the P3HT-OH film recorded at several positions in the negative GSB and positive PIA signatures. At all wavelengths, there is a fast biphasic decay of the intensity with time constants of 0.8 ps and 9.4 ps, pointing to rapid recombination of the excitations to the neutral ground state. There is also a very slow component everywhere in the TA spectrum, assigned to long-lived polarons and triplet excitons. It represents 13% and 6% of the initial signal magnitude of the GSB and PIA bands, respectively. The fast initial ground state recovery differs from the singlet exciton lifetime of 470 ps measured for P3HT polymer film by fluorescence up-conversion spectroscopy.[58] However, an important 8 ps decay component was also found in the PIA and SE signals recorded by TA spectroscopy with a pristine P3HT film.[65] It is probable that singlet exciton-exciton annihilation plays a role in the observed fast recombination, given the high excitation intensity (190 μJ/cm^2) used in our TA experiments. The high pump intensity was necessary due to the extremely small signal of the PCB-P3HT samples, which was mainly caused by a low film thickness and low absorbance (see sample preparation).

The TA spectra of PCB-P3HT drop cast from THF (micelle morphology) and from DCB (fibrous morphology) are illustrated in Fig. 8(b) and Fig. 8(c), respectively. It is immediately clear that they

show similar spectral features, which are distinctively different from the ones observed in the P3HT-OH film. In particular, there is a new positive band in the 610 nm to 780 nm region, present already at the earliest measurable timedelay of 150 fs. The same band appears when PCBM is blended with P3HT polymer in BHJ films, and it was assigned to mobile polarons that result from charge separation.[65, 67] The presence of the polaron band and absence of any SE even at the earliest timedelays evidences that quantitative CS occurs for PCB-P3HT film, and that it is ultrafast (< 150 fs). The dyad therefore behaves very differently in the solid state than in THF solution, where multiphasic, partial and relatively slow (average 100 ps) excitation energy transfer to the fullerene occurs. For the PCB-P3HT films cast from both solvents, PIA is also seen at higher wavelengths (860 nm to 1050 nm). The signal is weaker than in the P3HT-OH control compound. The near-infrared absorption mostly arises from charged species, although not necessarily from mobile polarons. In TA studies with P3HT:PCBM blends, several contributions were found in this region, such as PIA from localized P3HT polarons, from the PCBM anion (~1000 nm) and from polarons that are coulombically bound to the PCBM anion (intermediate charge transfer state).[65, 67] A contribution from the P3HT singlet state absorption at early timedelays due to slower CS components in annealed P3HT:PCBM films has also been suggested,[68] but probably plays only a minor role in PCB-P3HT films, given the absence of SE already at 150 fs.

The dynamics associated with the TA spectra of PCB-P3HT cast from THF and DCB are shown in Fig. 9(b) and Fig. 9(c), respectively. For both samples, an initial biphasic decay of the positive and negative signals is observed (mainly loss of charged species formed by ultrafast CS), followed by a slow component due to long-lived charge carriers, that appears as a plateau in the shown time window. The long-lived component in PCB-P3HT is much more important than for the control compound P3HT-OH, since many more charge carriers are generated by CS in the presence of the fullerene. A global analysis yields time constants of 0.8 ps and 30.1 ps for the fast decay in the THF sample. Comparable time constants of 0.6 ps and 21.5 ps are found for the fibrous sample cast from DCB. This fast loss of charge carriers could originate from monomolecular processes (geminate recombination in an initial charge transfer state, recombination caused by interfacial trap states) and/or from intensity-dependent processes (bimolecular recombination and exciton-charge annihilation, if there is a small

fraction of singlet excitons left that undergo slower quenching).[65, 68] The fast components of the ground state recovery increase when a higher excitation intensity (250 μJ/cm^2 versus 190 μJ/cm^2) is used, as shown with the dynamics around 500 nm (blue and black curves) for the PCB-P3HT film cast from THF in Fig. 9(b). Note that the effect is probably exaggerated, since the curves at the two intensities are scaled at the negative maximum around 0 ps, which also contains a contribution from intensity-dependent non-linear artifacts (cross-phase modulation). For this reason, the result could not be quantitatively exploited; nevertheless it indicates that excitation-intensity dependent recombination/annihilation plays a role in our measurements.

We initially expected that improved carrier delocalization and transport in the ordered fibrous morphology obtained by casting PCB-P3HT from DCB would increase the yield and lifetime of the long-lived charge carriers. Indeed, with the self-assembly proposed in Fig. 7(a), the holes can travel along the P3HT π-stacks, while the electrons hop along the phase separated fullerenes that surround the fibers. This mechanism is not possible in the micelles obtained from THF. The difference in morphology between the dyad samples cast from the two solvents is confirmed by the shape of the negative GSB band of the P3HT moiety below 600 nm (Fig. 8(b) and (c)). It is much more structured for DCB due to the important π-stacking of the P3HT chains in the ordered fibers. The absence of structure in the micelle absorption (which is easier to see in the GSB than the steady-state spectrum due to strong light scattering) confirms that the polymer chains are more amorphous in this morphology. However, when the dynamics of the GSB (500 nm, 550 nm) are compared for the dyad films cast from the two solvents in Fig. 9(b) and Fig. 9(c), it appears that the ground state recovery related to the two fast time constants is more pronounced for the fibrous compared to micellar morphology (there is a 66% and 48% loss of initial GSB intensity, respectively). The dynamics of mobile polarons can be followed at 700 nm for PCB-P3HT (Fig. 9(b) and Fig. 9(c)). In good agreement with the values obtained from the ground state recovery, 78% and 47% of those mobile charge carriers decay with the fast time constants in the DCB and THF films, respectively, while the rest is long-lived. This implies that fast charge carrier recombination to the neutral ground state is more important in the fibrous system.

It is plausible that the intensity-dependent recombination/annihilation is enhanced in the fibrous morphology, because the interacting species (charges, excitons) can move faster in the ordered π-stacked morphology. With the high excitation intensity of the femtosecond experiments, the concentration of the photoinduced species is very high (much higher than in operating solar cell conditions), so that their encounter rate is increased by higher mobility/diffusion in the crystalline material, leading to more charge carrier losses. Furthermore, we cannot exclude monomolecular recombination for PCB-P3HT and this might also affect the two morphologies differently. Geminate recombination from a bound intermediate charge transfer state, which absorbs in the near-infrared region (>800 nm), has been suggested for P3HT:PCBM blends based on TA experiments.[65, 68] Alternatively, recent work suggests that singly occupied interfacial trap states play an important role in monomolecular recombination to the ground state of polymer:fullerene blends, when an oppositely charged carrier reaches the trap.[69-73] In this view, the intermediate charge transfer state can be reinterpreted as a trap state.

In both interpretations, the PIA signal above 800 nm is ascribed to a state that leads to enhanced monomolecular recombination. Figure 8 shows that the relative magnitude of the PIA signal around 900 nm is increased at early timedelays for PCB-P3HT cast from DCB compared to THF, which could indicate a higher initial population of the bound charge transfer state or trap state, leading to more monomolecular recombination in the fibrous sample. The dynamics of the 900 nm band for both samples are shown in Fig. 9(b) and Fig. 9(c). It is especially clear for the THF sample that the mobile polaron band at 700 nm has a different dynamics than the band at 900 nm (the latter decays faster), confirming the different origin of the two PIA signatures. The important decay of the 900 nm band within the shown 400 ps time window reflects both monomolecular recombination from the charge transfer or trap state, as well as conversion of the bound or trapped charges to free charge carriers. It is interesting to observe that the fraction of very long-lived population absorbing at 900 nm is higher for the DCB sample than for the THF sample (20% versus 13%), indicating that the state responsible for monomolecular recombination remains active for a longer time.

In a previous TA study of non-annealed and annealed P3HT:PCBM BHJ blends, fast ground state recovery on the same time scale as the one observed here for PCB-P3HT was seen (with 9 ps in the non-annealed film and 4 ps in the annealed film).[65] Interestingly, the fraction of GSB decay on this time scale also increased from 41% to 66% when going from the non-annealed sample to the more ordered annealed sample with more P3HT π-stacking. Although the comparison has to be taken with care because the experimental conditions were different (490 nm excitation, lower pump intensity), this result points to a comparable loss of charge carriers (around 66%) in PCB-P3HT cast from DCB and in annealed P3HT:PCBM blends on the short time scale. As this loss is partly induced by the high excitation intensity used in femtosecond laser experiments, it might be less severe under operating solar cell conditions with much lower light intensity. In the previous publication,[65] the total fraction of long-lived charge carriers was still found to be larger in the annealed compared to the non-annealed P3HT:PCBM blends, because the amplitude of an additional 800 ps charge recombination component decreased with annealing.[65] We did not observe any 800 ps decay component or related effect for PCB-P3HT. Therefore, we conclude that the yield of long-lived mobile charge carriers is higher for the dyad film in the micelle morphology (cast from THF) than in the fibrous morphology (cast from DCB). In spite of the higher yield of long-lived charge carriers, the micelle morphology is expected to perform poorly in photovoltaic devices because of limited charge transport. Note that we cannot make a statement about the lifetime of the carriers in the μs/ms regime with our femtosecond experiments.

Finally, it should be mentioned that the PCB moiety of the dyad, not only the P3HT part, is excited with our TA experiments at 400 nm. This does not change any of the above interpretations, since fullerene excitation in the presence of a conjugated polymer also leads to ultrafast CS.[74] Even if some PCB singlet excitons remain after 150 fs, their contribution to the PIA spectra is expected to be insignificant, as only an extremely weak signal could be obtained for much thicker pure PCBM films in the same experimental conditions (data not shown). It should also be mentioned that the TA dynamics were measured at various positions of the relatively inhomogeneous drop-cast films and that small variations occurred. However, there was in no case a higher yield of long-lived polarons for the DCB-cast sample, in agreement with our conclusions.

IV. SUMMARY AND CONCLUSIONS

We reported here on the femtosecond spectroscopic characterization of a covalently linked dyad, PCB-P3HT, formed by a segment of the conjugated polymer P3HT (electron or energy donor) that is end-capped with the fullerene derivative PCB (electron or energy acceptor), derived from PCBM. Steady-state absorption spectroscopy in THF solution reveals weak electronic coupling and no charge transfer between the two moieties of the dyad in the ground state. The fluorescence of PCB-P3HT in solution stems only from the polymer chain and excitation of the fullerene part leads to no significant emission. The fluorescence quantum yield of the P3HT segment in THF is reduced by 64% if it is covalently attached to PCB, compared to the control compound P3HT-OH without linked fullerene. Fluorescence up-conversion measurements show that the partial fluorescence quenching is multiphasic with an average time constant of about 100 ps. Moreover, the time-resolved emission studies evidence early changes in the fluorescence spectrum due to excited-state relaxation processes (exciton hopping to lower energy, torsional rearrangements), which also occur in higher molecular weight P3HT polymer. The quenching and relaxation in the dyad occur on the same time scale and are therefore strongly entangled.

Transient absorption spectroscopy was carried out for P3HT-OH and PCB-P3HT in THF solution. The obtained spectra are surprisingly similar for both compounds and mainly show intersystem crossing from the singlet to the triplet state at long time delays. Nevertheless, the triplet state is populated in smaller yield in the dyad because of the additional quenching pathway, which could be assigned to singlet excitation energy transfer from the P3HT to the PCB moiety, based on faster ground state recovery of the P3HT segment in the dyad.

All the results obtained with the steady-state, fluorescence up-conversion and polarization-sensitive emission measurements confirm self-assembly of PCB-P3HT into micelles in THF, with no significant π-stacking between the P3HT chains. The micelle formation is due to the much higher solubility of P3HT compared to the fullerene moiety of the dyad in this solvent. Pure C_{60} can be incorporated into the fullerene-rich center of the micelles. This dramatically increases the solubility of C_{60} in THF, but does not lead to additional quenching between P3HT and the fullerenes inside the micelles.

Femtosecond transient absorption spectroscopy was carried out for P3HT-OH film drop-cast from THF and for PCB-P3HT film drop-cast from THF and DCB. The spectral signatures for P3HT-OH resemble the ones previously reported for P3HT polymer film. They are interpreted in terms of singlet excitons that decay with time constants of 0.8 ps and 9.4 ps, mainly due to intensity-induced processes. Long-lived components in the ground state bleach and photoinduced absorption bands are due to a small yield of polarons and triplet excitons.

The AFM picture of the PCB-P3HT sample cast from THF shows a micelle-like morphology (same self-assembly as in solution), while a network of π-stacked P3HT fibers surrounded by fullerenes is formed in the DCB-cast film. In the transient absorption spectra, the presence of structure in the ground state bleach band only for the fibrous film confirms the higher polymer ordering in this sample. Otherwise, the transient absorption signatures for the dyad films are quite similar for both casting solvents and distinctly different from the ones of P3HT-OH. The typical photoinduced absorption bands due to charged polarons, similar to the ones reported for P3HT:PCBM blends, appear around 700 nm within the 150 fs resolution of the instrumentation. Together with the absence of any stimulated emission, this confirms ultrafast quantitative charge separation in PCB-P3HT films.

The fraction of long-lived charge carriers in PCB-P3HT is much higher than in P3HT-OH, but there is still some loss of charge carriers that occurs with time constants of 0.6-0.8 ps and 20-30 ps. From the dynamics of the ground state bleach and of the mobile polaron absorption, we deduce that 47% and 66-87% of the charges recombine on this time scale for the THF and DCB samples, respectively. We discuss the origin of the loss in terms of pump intensity-dependent processes (bimolecular recombination and exciton-charge annihilation) as well as monomolecular processes (geminate recombination in an initial charge transfer state, recombination caused by interfacial trap states). The increased recombination in the fibrous sample cast from DCB can be explained by enhanced intensity-induced processes due to better transport properties in the ordered system, and by increased monomolecular recombination because the initial population and lifetime of the bound charge transfer state or trap state absorbing around 900 nm is higher.

Our initial expectation that improved transport in the fibers would increase the yield and lifetime of the polarons was therefore not met. Nevertheless, a very similar fast recombination of 66% of the charge carriers has been reported for an annealed P3HT:PCBM blend, which means that PCB-P3HT is not necessarily a worse candidate as an active material in organic solar cells. The loss of charge carriers can also be expected to be lower with the lower excitation intensity used in operating solar cells. Furthermore, the covalent linkage of the P3HT and PCB moieties together with the high degree of ordering offer a way to control the donor-acceptor heterojunction.

[1] C. W. Tang, Appl. Phys. Lett. **48**, 183 (1986).
[2] B. C. Thompson and J. M. J. Frechet, Angew. Chem., Int. Ed. Engl. **47**, 58 (2008).
[3] W. Ma, C. Yang, X. Gong, K. Lee, and A. J. Heeger, Adv. Funct. Mater. **15**, 1617 (2005).
[4] C. J. Brabec, N. S. Sariciftci, and J. C. Hummelen, Adv. Funct. Mater. **11**, 15 (2001).
[5] G. Yu, J. Gao, J. C. Hummelen, F. Wudl, and A. J. Heeger, Science (Washington, DC, U. S.) **270**, 1789 (1995).
[6] N. Banerji, G. Duvanel, A. Perez-Velasco, S. Maity, N. Sakai, S. Matile, and E. Vauthey, J. Phys. Chem. A **113**, 8202 (2009).
[7] N. Sakai, A. L. Sisson, S. Bhosale, A. Fuerstenberg, N. Banerji, E. Vauthey, and S. Matile, Org. Biomol. Chem. **5**, 2560 (2007).
[8] S. Bhosale, et al., Science (Washington, DC, U. S.) **313**, 84 (2006).
[9] W.-S. Li, K. S. Kim, D.-L. Jiang, H. Tanaka, T. Kawai, J. H. Kwon, D. Kim, and T. Aida, J. Am. Chem. Soc. **128**, 10527 (2006).
[10] G. Kodis, Y. Terazono, P. A. Liddell, J. Andréasson, V. Garg, M. Hambourger, T. A. Moore, A. L. Moore, and D. Gust, J. Am. Chem. Soc. **128**, 1818 (2006).
[11] M. R. Wasielewski, J. Org. Chem. **71**, 5051 (2006).
[12] D. M. Guldi, G. M. A. Rahman, F. Zerbetto, and M. Prato, Acc. Chem. Res. **38**, 871 (2005).

[13] H. Imahori, D. M. Guldi, K. Tamaki, Y. Yoshida, C. P. Luo, Y. Sakata, and S. Fukuzumi, J. Am. Chem. Soc. **123**, 6617 (2001).

[14] N. Sakai, R. Bhosale, D. Emery, J. Mareda, and S. Matile, J. Am. Chem. Soc. **132**, 6923 (2010).

[15] S. Maity, R. Bhosale, N. Banerji, E. Vauthey, N. Sakai, and S. Matile, Org. Biomol. Chem. **8**, 1052 (2010).

[16] A. L. Sisson, N. Sakai, N. Banerji, A. Furstenberg, E. Vauthey, and S. Matile, Angew. Chem., Int. Ed. Engl. **47**, 3727 (2008).

[17] M. Morisue, S. Yamatsu, N. Haruta, and Y. Kobuke, Chem. Eur. J. **11**, 5563 (2005).

[18] D. M. Guldi, G. M. A. Rahman, M. Prato, N. Jux, S. H. Qin, and W. Ford, Angew. Chem., Int. Ed. **44**, 2015 (2005).

[19] D. M. Guldi, J. Phys. Chem. B **109**, 11432 (2005).

[20] D. M. Guldi and M. Prato, Chem. Commun., 2517 (2004).

[21] F. B. Abdelrazzaq, R. C. Kwong, and M. E. Thompson, J. Am. Chem. Soc. **124**, 4796 (2002).

[22] Y. Yamamoto, et al., Science (Washington, DC, U. S.) **314**, 1761 (2006).

[23] F. Würthner, et al., J. Am. Chem. Soc. **126**, 10611 (2004).

[24] L. Schmidt-Mende, A. Fechtenkotter, K. Mullen, E. Moons, R. H. Friend, and J. D. MacKenzie, Science (Washington, DC, U. S.) **293**, 1119 (2001).

[25] T. Nakamura, Y. Araki, O. Ito, K. Takimiya, and T. Otsubo, J. Phys. Chem. A **112**, 1125 (2008).

[26] T. Nishizawa, K. Tajima, and K. Hashimoto, J. Mater. Chem. **17**, 2440 (2007).

[27] M. Narutaki, K. Takimiya, T. Otsubo, Y. Harima, H. M. Zhang, Y. Araki, and S. Ito, J. Org. Chem. **71**, 1761 (2006).

[28] J. Roncali, Chem. Soc. Rev. **34**, 483 (2005).

[29] P. A. van Hal, J. Knol, B. M. W. Langeveld-Voss, S. C. J. Meskers, J. C. Hummelen, and R. A. J. Janssen, J. Phys. Chem. A **104**, 5974 (2000).

[30] E. Peeters, P. A. van Hal, J. Knol, C. J. Brabec, N. S. Sariciftci, J. C. Hummelen, and R. A. J. Janssen, J. Phys. Chem. B **104**, 10174 (2000).

[31] M. Fujitsuka, O. Ito, T. Yamashiro, Y. Aso, and T. Otsubo, J. Phys. Chem. A **104**, 4876 (2000).

[32] A. Cravino, Polym. Int. **56**, 943 (2007).

[33] A. Cravino and N. S. Sariciftci, J. Mater. Chem. **12**, 1931 (2002).

[34] A. Cravino, G. Zerza, M. Maggini, S. Bucella, M. Svensson, M. R. Andersson, H. Neugebauer, and N. S. Sariciftci, Chem. Commun., 2487 (2000).

[35] A. Cravino, et al., J. Phys. Chem. B **106**, 70 (2002).

[36] A. M. Ramos, M. T. Rispens, J. K. J. van Duren, J. C. Hummelen, and R. A. J. Janssen, J. Am. Chem. Soc. **123**, 6714 (2001).

[37] F. L. Zhang, M. Svensson, M. R. Andersson, M. Maggini, S. Bucella, E. Menna, and O. Inganas, Adv. Mater. (Weinheim, Ger.) **13**, 1871 (2001).

[38] F. Ouhib, A. Khoukh, J. B. Ledeuil, H. Martinez, J. Desbrieres, and C. Dagron-Lartigau, Macromolecules **41**, 9736 (2008).

[39] U. Stalmach, B. de Boer, C. Videlot, P. F. van Hutten, and G. Hadziioannou, J. Am. Chem. Soc. **122**, 5464 (2000).

[40] B. de Boer, U. Stalmach, P. F. van Hutten, C. Melzer, V. V. Krasnikov, and G. Hadziioannou, Polymer **42**, 9097 (2001).

[41] C. Yang, J. K. Lee, A. J. Heeger, and F. Wudl, J. Mater. Chem. **19**, 5416 (2009).

[42] F. Richard, C. Brochon, N. Leclerc, D. Eckhardt, T. Heiser, and G. Hadziioannou, Macromol. Rapid Commun. **29**, 885 (2008).

[43] R. C. Hiorns, E. Cloulet, E. Ibarboure, A. Khoukh, H. Bejbouji, L. Vignau, and H. Cramail, Macromolecules **43**, 6033 (2010).

[44] K. Sivula, Z. T. Ball, N. Watanabe, and J. M. J. Frechet, Advanced Materials **18**, 206 (2006).

45 F. Giacalone, J. L. Segura, N. Martin, J. Ramey, and D. M. Guldi, Chemistry-a European Journal **11**, 4819 (2005).

46 N. Martin, F. Giacalone, J. L. Segura, and D. M. Guldi, Synth. Met. **147**, 57 (2004).

47 B. W. Boudouris, F. Molins, D. A. Blank, C. D. Frisbie, and M. A. Hillmyer, Macromolecules **42**, 4118 (2009).

48 J. Y. Kim, S. H. Kim, H. H. Lee, K. Lee, W. L. Ma, X. Gong, and A. J. Heeger, Adv. Mater. (Weinheim, Ger.) **18**, 572 (2006).

49 M. Reyes-Reyes, K. Kim, and D. L. Carroll, Appl. Phys. Lett. **87**, 083506 (2005).

50 G. Li, V. Shrotriya, J. S. Huang, Y. Yao, T. Moriarty, K. Emery, and Y. Yang, Nat. Mater. **4**, 864 (2005).

51 H. Sirringhaus, et al., Nature **401**, 685 (1999).

52 M. Wang, A. J. Heeger, and F. Wudl, Small **7**, 298 (2011).

53 J. U. Lee, J. W. Jung, T. Emrick, T. P. Russell, and W. H. Jo, J. Mater. Chem. **20**, 3287 (2010).

54 N. Banerji, S. Cowan, M. Leclerc, E. Vauthey, and A. J. Heeger, J. Am. Chem. Soc. **132**, 17459 (2010).

55 A. Morandeira, L. Engeli, and E. Vauthey, J. Phys. Chem. A **106**, 4833 (2002).

56 A. Furstenberg and E. Vauthey, J. Phys. Chem. B **111**, 12610 (2007).

57 J. Clark, C. Silva, R. H. Friend, and F. C. Spano, Phys. Rev. Lett. **98**, 206406 (2007).

58 N. Banerji, S. Cowan, E. Vauthey, and A. J. Heeger, J. Phys. Chem. C **115**, 9726 (2011).

59 S. Cook, A. Furube, and R. Katoh, Energy Environ. Sci. **1**, 294 (2008).

60 T. W. Ebbesen, K. Tanigaki, and S. Kuroshima, Chem. Phys. Lett. **181**, 501 (1991).

61 X. M. Jiang, R. Osterbacka, O. Korovyanko, C. P. An, B. Horovitz, R. A. J. Janssen, and Z. V. Vardeny, Adv. Funct. Mater. **12**, 587 (2002).

62 R. Osterbacka, C. P. An, X. M. Jiang, and Z. V. Vardeny, Synth. Met. **116**, 317 (2001).

63 R. Osterbacka, C. P. An, X. M. Jiang, and Z. V. Vardeny, Science (Washington, DC, U. S.) **287**, 839 (2000).

64 M. Logdlund, R. Lazzaroni, S. Stafstrom, W. R. Salaneck, and J. L. Bredas, Phys. Rev. Lett. **63**, 1841 (1989).

65 I. W. Hwang, D. Moses, and A. J. Heeger, J. Phys. Chem. C **112**, 4350 (2008).

66 C. X. Sheng, M. Tong, S. Singh, and Z. V. Vardeny, Phys. Rev. B **75**, 085206 (2007).

67 J. M. Guo, H. Ohkita, H. Benten, and S. Ito, J. Am. Chem. Soc. **132**, 6154 (2010).

68 I. A. Howard, R. Mauer, M. Meister, and F. Laquai, J. Am. Chem. Soc. **132**, 14866 (2010).

69 S. R. Cowan, W. L. Leong, N. Banerji, G. Dennler, and A. J. Heeger, Adv. Funct. Mater. **in press** (2011).

70 W. Lin Leong, S. R. Cowan, and A. J. Heeger, Advanced Energy Materials **published online** (2011).

71 S. Cowan, A. Roy, and A. J. Heeger, Phys. Rev. B **82**, 245207 (2010).

72 R. A. Street, S. R. Cowan, and A. J. Heeger, Phys. Rev. B **82**, 121301 (2010).

73 R. A. Street, M. Schoendorf, J. Y. Lee, and A. Roy, Phys. Rev. B **81**, 205307 (2010).

74 M. M. Wienk, J. M. Kroon, W. J. H. Verhees, J. Knol, J. C. Hummelen, P. A. van Hal, and R. A. J. Janssen, Angew. Chem., Int. Ed. **42**, 3371 (2003).
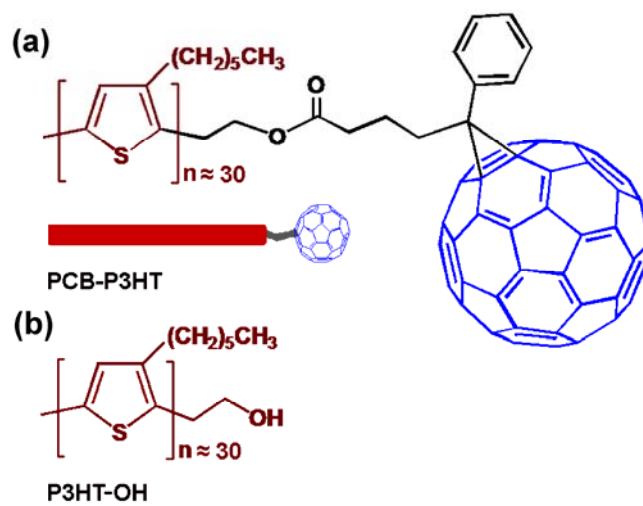
FIG. 1. Molecular structure (a) of PCB-P3HT together with a schematic representation of the molecule and (b) of P3HT-OH.
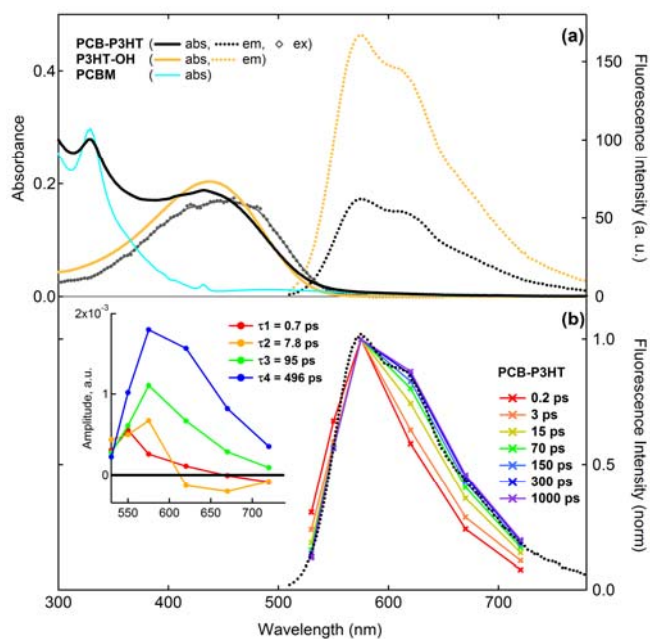
FIG. 2. (a) Steady-state absorption spectra (solid lines), emission spectra (dotted lines) and fluorescence excitation spectrum (line with markers) of PCB-P3HT (black), P3HT-OH (orange) and PCBM (light blue) in THF solution. (b) Normalized time-resolved emission spectra of PCB-P3HT in THF solution (2 mg/mL) after excitation at 500 nm, reconstructed from the global analysis of the femtosecond fluorescence time profiles at several emission wavelengths. The inset sows the decay-associated amplitude spectra.
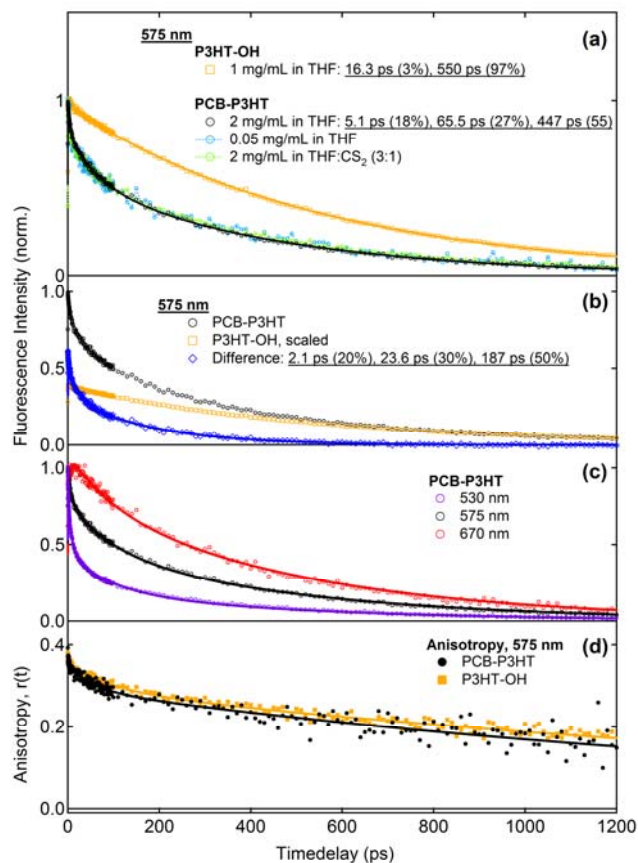
FIG. 3. (a) Ultrafast fluorescence time profiles following 500 nm excitation recorded at 575 nm for PCB-P3HT and P3HT-OH solution (see legend for solvents and concentration). (b) Difference between the scaled fluorescence time profiles obtained at 575 nm for PCB-P3HT (2 mg/mL) and P3HT-OH (1 mg/mL) in THF solution. (c) Fluorescence time profiles recorded at various emission wavelengths for PCB-P3HT in THF (2 mg/mL). (d) Time evolution of the fluorescence polarization anisotropy probed at 575 nm after 500 nm excitation of PCB-P3HT (2 mg/mL) and P3HT-OH (1 mg/mL) in THF solution.
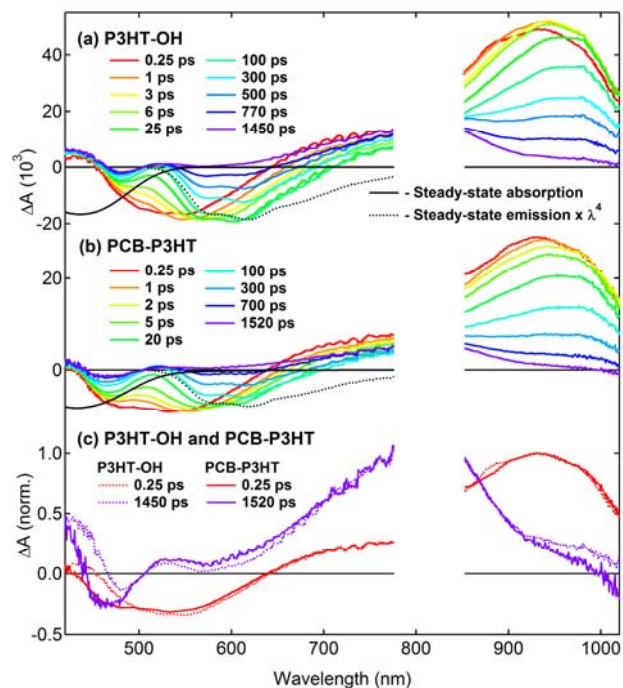
FIG. 4. Transient absorption spectra recorded at various timedelays after 400 nm excitation for (a) P3HT-OH in THF solution (0.5 mg/mL), (b) PCB-P3HT in THF solution (0.5 mg/mL). The black curves represent the steady-state absorption spectra, while the black dotted curves show the steady-state emission spectra (negative, a.u.). In (c) the normalized TA spectra of P3HT-OH and PCB-P3HT are compared for a short and a long timedelay.
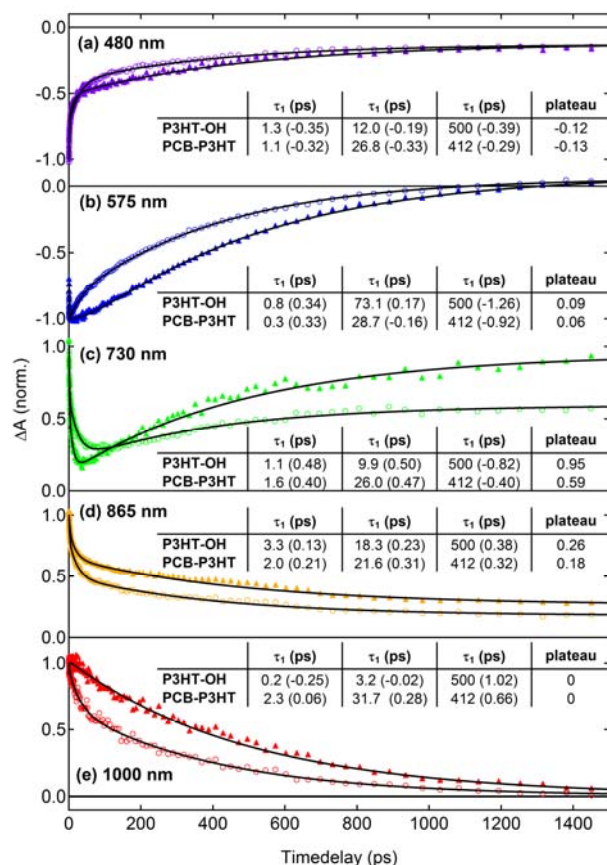
FIG. 5. Transient absorption dynamics recorded at various wavelengths after 400 nm excitation for P3HT-OH in THF solution (0.5 mg/mL, full triangles) and PCB-P3HT in THF solution (0.5 mg/mL, empty circles). The solid black lines represent the best multi-exponential fit. The fitting parameters (time constants and absolute amplitudes obtained with the normalized dynamics) are shown in the inset tables.
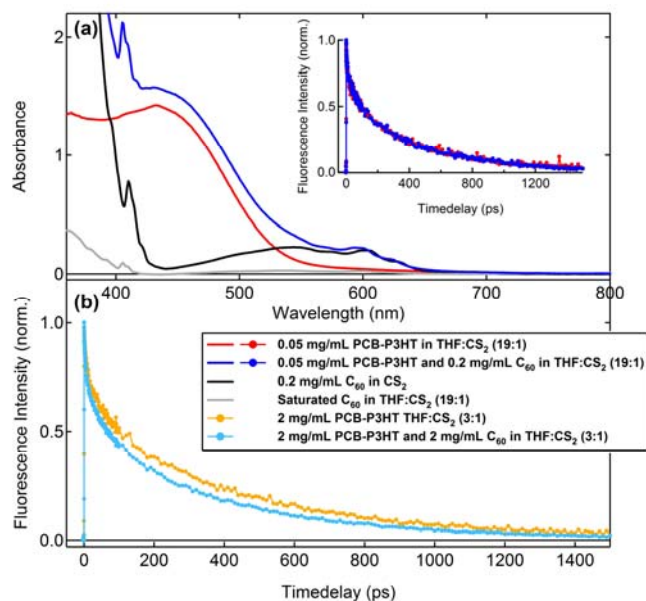
(a) 480 nm

	τ_1 (ps)	τ_1 (ps)	τ_1 (ps)	plateau
P3HT-OH	1.3 (-0.35)	12.0 (-0.19)	500 (-0.39)	-0.12
PCB-P3HT	1.1 (-0.32)	26.8 (-0.33)	412 (-0.29)	-0.13

(b) 575 nm

	τ_1 (ps)	τ_1 (ps)	τ_1 (ps)	plateau
P3HT-OH	0.8 (0.34)	73.1 (0.17)	500 (-1.26)	0.09
PCB-P3HT	0.3 (0.33)	28.7 (-0.16)	412 (-0.92)	0.06

(c) 730 nm

	τ_1 (ps)	τ_1 (ps)	τ_1 (ps)	plateau
P3HT-OH	1.1 (0.48)	9.9 (0.50)	500 (-0.82)	0.95
PCB-P3HT	1.6 (0.40)	26.0 (0.47)	412 (-0.40)	0.59

(d) 865 nm

	τ_1 (ps)	τ_1 (ps)	τ_1 (ps)	plateau
P3HT-OH	3.3 (0.13)	18.3 (0.23)	500 (0.38)	0.26
PCB-P3HT	2.0 (0.21)	21.6 (0.31)	412 (0.32)	0.18

	τ_1 (ps)	τ_1 (ps)	τ_1 (ps)	plateau
P3HT-OH	0.2 (-0.25)	3.2 (-0.02)	500 (1.02)	0
PCB-P3HT	2.3 (0.06)	31.7 (0.28)	412 (0.66)	0

(e) 1000 nm

ΔA (norm.)

Timedelay (ps)

FIG. 6. (a) Steady-state absorption spectra of PCB-P3HT (red), PCB-P3HT with C_{60} (blue), and a saturated solution of C_{60} (gray) in a THF:CS_2 solvent mixture (19:1 by volume), and of C_{60} in pure CS_2 (black). The concentrations are shown in the legend. The inset shows the fluorescence time profiles of the first two solutions recorded at 575 nm after excitation at 500 nm. (b) Fluorescence time profiles of a more concentrated solution of PCB-P3HT (2 mg/mL) without (orange) and with 2 mg/mL C_{60} (light blue) in a 3:1 THF:CS_2 mixture.
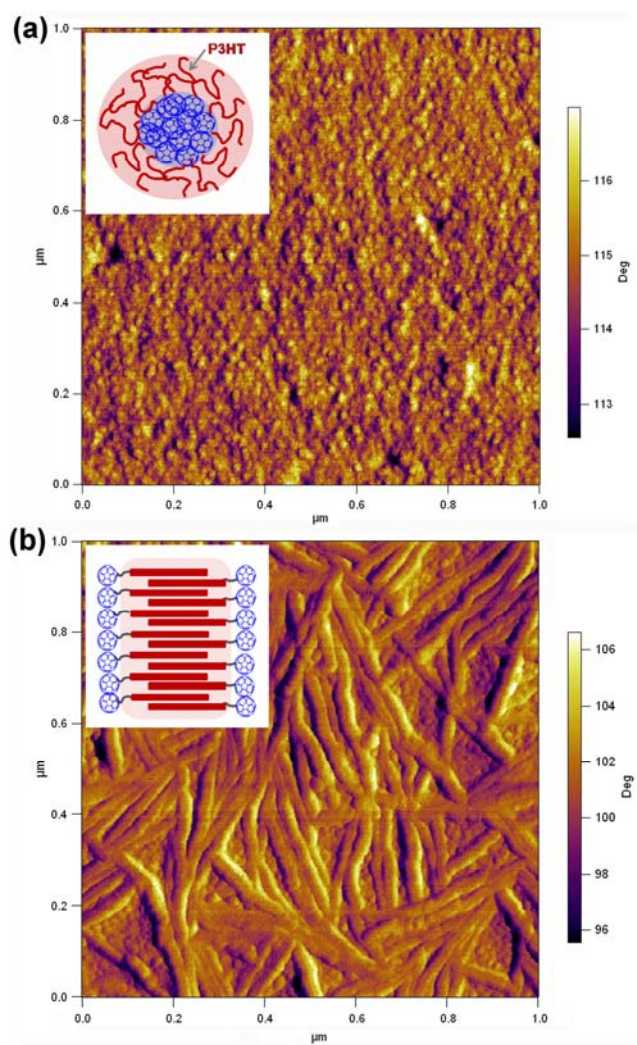
FIG. 7. AFM images (phase, on sapphire) of PCB-P3HT drop cast from (a) THF (2.0 mg/mL) and (b) DCB (12 mg/mL). The insets show a schematic representation of the proposed self-assembly.
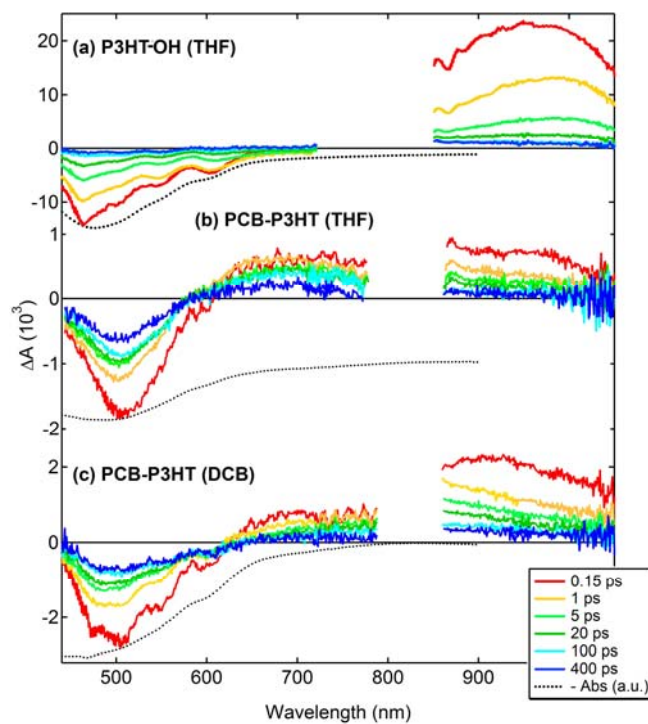
FIG. 8. Transient absorption spectra recorded at various timedelays after 400 nm excitation for (a) P3HT-OH drop-cast from THF (2 mg/mL), (b) PCB-P3HT drop-cast from THF (2 mg/mL), and (c) PCB-P3HT drop-cast from DCB (12 mg/mL). The black dotted curves represent the steady-state absorption spectra (negative, a.u.).
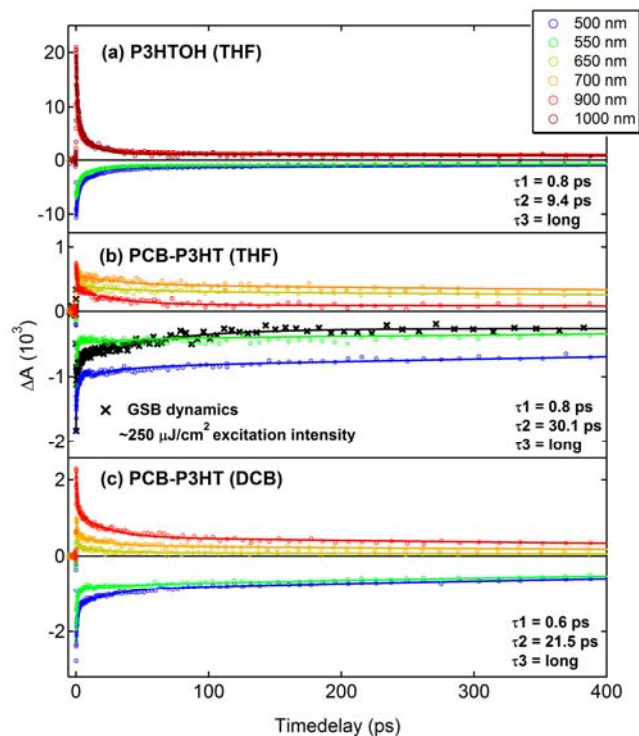
FIG. 9. Transient absorption dynamics recorded at various wavelengths after 400 nm excitation with 190 μJ/cm^2 for (a) P3HT-OH drop-cast from THF (2 mg/mL), (b) PCB-P3HT drop-cast from THF (2 mg/mL), and (c) PCB-P3HT drop-cast from DCB (12 mg/mL). The solid lines represent the best multi-exponential global fit.